

An electronic band sculpted by oxygen vacancies and indispensable for dilute superconductivity

Benoît Fauqué¹, Clément Collignon^{1,2,*}, Hyeok Yoon^{3,4,†}, Ravi², Xiao

Lin^{2,‡}, Igor I. Mazin⁵, Harold Y. Hwang^{3,4}, and Kamran Behnia²

(1) JEIP (USR 3573 CNRS), Collège de France, 75005 Paris, France

(2) Laboratoire de Physique et d'Etude de Matériaux (CNRS)
ESPCI Paris, Université PSL, 75005 Paris, France

(3) Stanford Institute for Materials and Energy Sciences,

SLAC National Accelerator Laboratory, Menlo Park, Stanford, California 94025, USA

(4) Department of Applied Physics, Stanford University, Stanford, California 94305, USA

(5) Department of Physics and Astronomy and Quantum Science and Engineering Center,
George Mason University, Fairfax, Virginia 22030, USA

(Dated: March 1, 2023)

Dilute superconductivity survives in bulk strontium titanate when the Fermi temperature falls well below the Debye temperature. Here, we show that the onset of the superconducting dome is dopant-dependent. When mobile electrons are introduced by removing oxygen atoms, the superconducting transition survives down to $2 \times 10^{17} \text{ cm}^{-3}$, but when they are brought by substituting Ti with Nb, the threshold density for superconductivity is an order of magnitude higher. Our study of quantum oscillations reveals a difference in the band dispersion between the dilute metals made by these doping routes and our band calculations demonstrate that the rigid band approximation does not hold when mobile electrons are introduced by oxygen vacancies. We identify the band sculpted by these vacancies as the exclusive locus of superconducting instability in the ultra-dilute limit.

I. Introduction

Discovered half a century ago [1], superconductivity in strontium titanate is attracting renewed attention [2, 3]. It lies beyond the Migdal-Eliashberg [4] framework, since the Fermi temperature of electrons falls below the Debye temperature of phonons [5, 6]. The dilute metal going through this superconducting instability has non-trivial transport properties [7–10]. The insulating parent, identified as a quantum paraelectric [11], due to its huge permittivity, displays an unusual low-temperature thermal conductivity [12] and a puzzling thermal Hall effect [13]. Soft transverse optical phonons, hybridizing with transverse acoustic phonons at low temperatures [14, 15], are suspected to play a major role in this solid.

The proximity to a ferroelectric instability is often invoked in explaining superconductivity [16–18]. Several experimental studies have documented a constructive interplay between superconductivity and ferroelectricity [19–22] and recent theoretical accounts of Cooper pairing invoke the exchange of two [23–25] or one [26, 27] soft phonons between pairing electrons. A two-phonon exchange scenario, first invoked decades ago [28], leads to instantaneous electron-electron attraction and can explain [24] the experimentally-observed persistence of superconductivity at densities below 10^{18} cm^{-3} [5, 29].

Here, we present a study of superconducting transition and quantum oscillations in oxygen-reduced and Nb-substituted strontium titanate in the dilute limit. We find that when $n < 5 \times 10^{18} \text{ cm}^{-3}$, superconductivity is present in $\text{SrTiO}_{3-\delta}$, but absent in $\text{SrTi}_{1-x}\text{Nb}_x\text{O}_3$, either single-crystalline or custom-made thin films. The dilute metals generated by these alternative doping routes are also different. Compared to $\text{SrTiO}_{3-\delta}$, $\text{SrTi}_{1-x}\text{Nb}_x\text{O}_3$ has a less spherical Fermi surface and hosts lighter electrons. Moreover, the Lifshitz transition occurs at a lower density. We present numerical evidence that the virtual crystal approximation used in the LDA band calculations [30] holds for Nb doping, but not for oxygen deficiency. We conclude that while both doping routes generate a superconducting ground state, dilute superconductivity (arising in a metal where e-e distance is of the order 10 nm) occurs only when the occupied band is sculpted by oxygen vacancies. A larger coupling between the electrons of the vacancy-sculpted band and soft TO phonons, or a larger electronic density of states, or a combination of both, may be the origin.

SrTiO_3 can be n-doped by a variety of atomic substitutions. The focus of the present study is to compare substitution of tetravalent Ti^{4+} by pentavalent Nb^{5+} with creation of oxygen vacancies. While both lead to n-doping, there is no *a priori* reason to believe that they affect the electronic structure in the same way [32]. In presence of an O vacancy, the two neighboring Ti ions are left with one extra electron each. What can happen with these electrons? They can either get collectively extended over all Ti sites or both occupy the vacancy. In a recent DFT+DMFT calculation, Souto-Casares, Spaldin and Ederer [33] found that if the Hubbard repulsion on Ti and the concentration are both large, one or even

* Present address: Department of Physics, Massachusetts Institute of Technology, Cambridge, Massachusetts 02139, USA

† Present address: Department of Physics, University of Maryland, College Park, Maryland 20742, USA

‡ Present address: School of Science, Westlake University, 18 Shilongshan Road, 310024 Hangzhou, China

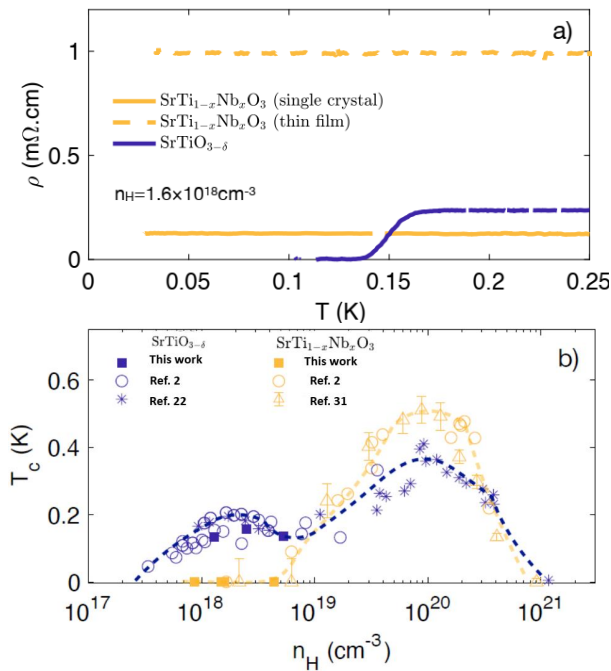


FIG. 1. **Different thresholds for emergence of superconductivity:** a) Temperature dependence of electrical resistivity (ρ_{xx}) in SrTi_{1-x}Nb_xO₃ and SrTiO_{3- δ} (orange) sample with similar carrier density $n_H \simeq 1.6 \times 10^{18} \text{ cm}^{-3}$. Neither the thin film nor the single crystalline SrTi_{1-x}Nb_xO₃ shows a superconducting transition at this carrier density. b) Doping evolution of the superconducting critical temperature (T_c). Solid symbols represent samples studied in the present work. Open symbols represent what was reported previously [2, 22, 31].

two electrons will prefer to avoid the Hubbard repulsion on Ti and “hide” in the vacancy. However, the effective concentration of vacancies in that work [33] was one per four formula units, which is several orders of magnitude higher than the relevant experimental range. At very small concentrations, Hubbard correlation between the doped electrons, included in the DMFT method and not in the DFT, are much less important than geometric changes such as lattice relaxation. Keeping this in mind, we have performed full structural relaxation in the density functional theory (DFT), using an $8 \times 8 \times 8$ supercell of 64 f.u., and either replacing one Ti with Nb or removing one O. As discussed below, we found that the resulting electronic structure near the bottom of the conduction band is dramatically different in the two cases.

II. Results

A. Dopant dependent superconductivity

Fig.1a shows the low-temperature electrical resistivity (ρ_{xx}) of three samples with the same Hall carrier density.

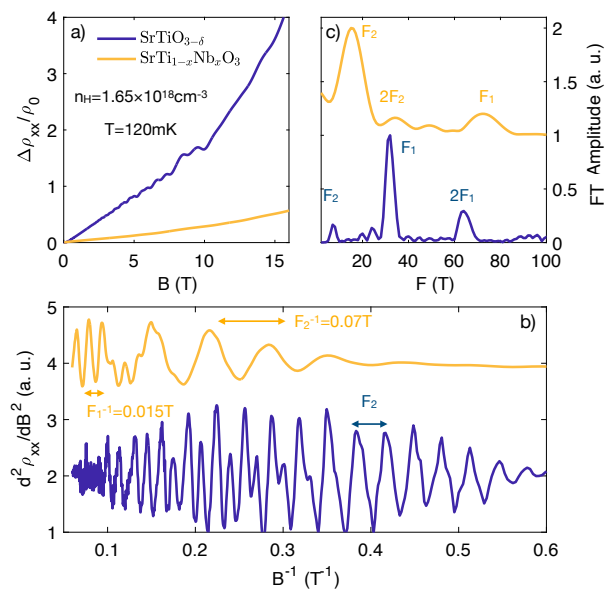


FIG. 2. **Distinct Fermi surfaces:** a) Magnetoresistance ($\frac{\Delta\rho_{xx}}{\rho_0}$) vs B in SrTi_{1-x}Nb_xO₃ (orange) and SrTiO_{3- δ} (blue) with the same Hall carrier density $n_H = 1.65 \times 10^{18} \text{ cm}^{-3}$ at $T = 120 \text{ mK}$. b) Traces of the quantum oscillations in $\frac{\partial^2\rho_{xx}}{\partial B^2}$ as function of B^{-1} for both samples. c) Amplitude of the Fourier transform (FT) vs frequency (F) deduced from b). The amplitude was normalized by the peak value and shift for clarity. In both samples, two frequencies (and their harmonics) can be identified, respectively labelled F_1 and F_2 .

One can see that SrTiO_{3- δ} becomes a superconductor, but not SrTi_{1-x}Nb_xTiO₃ (at least not down to 30mK). Note that, the oxygen deficient sample has a residual resistivity lower than the thin film and larger than the crystalline SrTi_{1-x}Nb_xTiO₃. This rules out disorder as the driver of this dichotomy. Studying four different Nb-doped SrTiO₃ thin films [34] with a thickness of $\approx 900 \text{ nm}$ and nominal Nb concentrations of 0.02 and 0.04 atomic percent, we found that none was superconducting (See the supplement for more details about samples and data [35]).

Fig.1.b draws the superconducting phase diagram of SrTiO_{3- δ} and in SrTi_{1-x}Nb_xTiO₃ according to the available data reported by different groups [2, 22, 31]. The critical temperature does not evolve identically. The peak in T_c of the principal dome is higher in Nb-doped strontium titanate, while a lower superconducting dome is present for SrTiO_{3- δ} and absent in SrTi_{1-x}Nb_xO₃.

Evidence for superconductivity in this density range is limited to the detection of zero resistivity. The critical temperature of bulk probes of superconductivity, such as specific heat [36], thermal conductivity [36] and diamagnetism [37] is consistently lower than the temperature at which resistivity drops to zero. Given the strong variation of critical temperature with pressure or strain [18], this points to the survival of filamentary superconductiv-

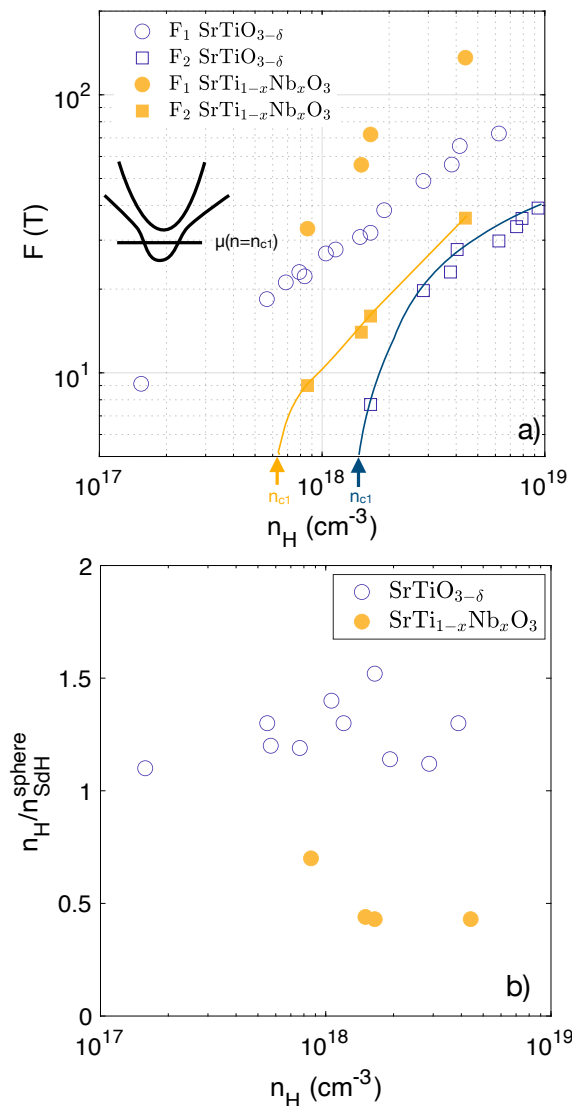


FIG. 3. **Doping evolution of the Fermi surface of $\text{SrTi}_{1-x}\text{Nb}_x\text{O}_3$ and $\text{SrTiO}_{3-\delta}$** : a) Frequencies of the quantum oscillations of the two sub-bands F_1 (circles) and F_2 (squares) vs. the Hall carrier density (n_H) in $\text{SrTi}_{1-x}\text{Nb}_x\text{O}_3$ and in $\text{SrTiO}_{3-\delta}$ [29]. The Lifshitz transition occurs at different threshold densities. b) Ratio of the carrier density extracted from quantum oscillations frequency assuming two spherical pockets. A difference persists in all samples. This implies distinct geometries for the Fermi surface in the two cases.

ity with a higher critical temperature at specific locations like dislocations or domain boundaries. Nevertheless, oxygen-reduced samples display bulk superconductivity for a carrier density as low as $4.5 \times 10^{18} \text{cm}^{-3}$ [19, 22] and the Nb-substituted ones do not show any transition (resistive or else) at this concentration. Therefore, there is a genuine difference of the ground states, irrespective of the origin of filamentary superconductivity.

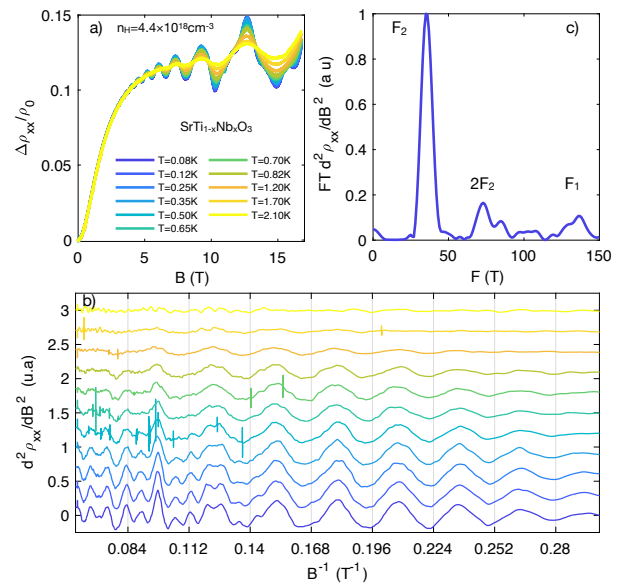


FIG. 4. **Quantum oscillations in $\text{SrTi}_{1-x}\text{Nb}_x\text{O}_3$ with $n_H = 4.4 \times 10^{18} \text{cm}^{-3}$** : a) $\frac{\Delta \rho_{xx}}{\rho_0}$ vs B at different temperatures from 80 mK to 2.1 K. b) $\frac{\partial^2 \rho_{xx}}{\partial B^2}$ as a function of B^{-1} displaying quantum oscillations. c) FT of the data at $T = 80$ mK.

B. Dopant dependent metallicity

Let us now compare the normal state of these two dilute metals. Structurally, the distribution of oxygen vacancies is known to be less homogeneous than the distribution of Nb atoms [38]. However, in both cases, electrons belong to a single Fermi sea (and not to a plurality of puddles). Since the Bohr radius is as long as several hundreds of nanometer [39], disorder is averaged over a volume containing many dopants. In both oxygen-reduced and Nd-substituted strontium titanate, the carrier mean-free-path is much longer than the interdopant distance and quantum oscillations are visible at moderate (≈ 2 T) magnetic fields.

We carried out a careful examination of the structure of the Fermi surface by looking at the Shubnikov-de Haas effect in the two cases. Magnetoresistance ($\frac{\Delta \rho_{xx}}{\rho_0}$) at $T = 120$ mK and for $B \parallel [001]$ (See Fig.2a)) reveals a difference. Quantum oscillations are visible on top of a monotonic background in both. As seen in Fig.2b, however, despite the quasi-equality of their Hall carrier density, the second derivative of resistivity $\frac{\partial^2 \rho_{xx}}{\partial B^2}$ shows different patterns. Two main frequencies, labelled F_1 and F_2 can be resolved, in qualitative agreement with previous studies of quantum oscillations [5, 40, 41]. However, F_1 and F_2 are not identical in the two cases, implying a difference in the structure of the Fermi surface between superconducting $\text{SrTiO}_{3-\delta}$ and non-superconducting $\text{SrTi}_{1-x}\text{Nb}_x\text{TiO}_3$.

By studying three other Nb-doped thin-film samples with n_H ranging from $8.6 \times 10^{17} \text{cm}^{-3}$ to $4.4 \times 10^{18} \text{cm}^{-3}$ (see [35] for sample details), we found that the evolu-

tion of F_1 and F_2 in $\text{SrTi}_{1-x}\text{Nb}_x\text{O}_3$ and in SrTiO_{3-x} [29] are not identical (See Fig. 3.a). At a given Hall carrier density, both frequencies are larger in $\text{SrTi}_{1-x}\text{Nb}_x\text{O}_3$ compared to $\text{SrTiO}_{3-\delta}$ (See the supplement [35] for more details on the analysis).

In the absence of an angle-dependent study, possible multiplicity of structural domains below 105 K is a source of complication. In multi-domain samples the orientation of magnetic field can be perpendicular or parallel to the c -axis according to the orientation of domains. However, a simple procedure reveals a difference in Fermi surface geometry in the two cases. Assuming that the two sub-bands are isotropic, the carrier density can be deduced from the frequencies of quantum oscillations: $n_{SDH}^{sphere} = \frac{1}{3\pi^2} \left(\left(\frac{2eF_1}{\hbar} \right)^{3/2} + \left(\frac{2eF_2}{\hbar} \right)^{3/2} \right)$ and then compared to the Hall carrier density, n_H . Their ratio, $\frac{n_H}{n_{SDH}^{sphere}}$, is a measure of the deviation of the pockets from perfect spheres. Fig. 3.b compares the two cases at different doping levels. The ratio is ≈ 1.2 in $\text{SrTiO}_{3-\delta}$ and ≈ 0.5 in $\text{SrTi}_{1-x}\text{Nb}_x\text{O}_3$. Thus, the Fermi surface of Nb-doped samples is less spherical than the Fermi surface of $\text{SrTi}_{1-x}\text{Nb}_x\text{O}_3$. Moreover, as seen in Fig. 3.a, the threshold for filling the second band, i.e. the onset of the Lifshitz transition is also lower in the Nb-doped case.

We note that F_1 and F_2 of our Nb-doped samples are in good agreement with what has been found in La-doped samples [41]. This suggests that the Fermi surface in La-doped and in Nb-doped strontium titanate are similar. Interestingly, there is no report of a superconducting transition in single crystals [20] or thin films of $\text{Sr}_{1-x}\text{La}_x\text{TiO}_3$ [21] when the carrier density at very low ($\approx 10^{18} \text{ cm}^{-3}$) doping.

By studying the temperature dependence of the quantum oscillations and using the Lifshitz-Kosevitch formalism, we extracted the cyclotron mass of electrons. Fig. 4 shows the quantum oscillations and their temperature dependence in the sample with highest carrier concentration ($n_H = 4.4 \times 10^{18} \text{ cm}^{-3}$). The results of the analysis are shown in the upper panel of Fig. 4c). We find an effective mass of $m^* = 1.4 \pm 0.1m_0$ for the lower band, comparable to the value found previous studies of Nb-doped [40] (and La-doped [41]) strontium titanate. In contrast, the effective mass of the lower band in the oxygen-reduced case at this carrier density is $m^* = 1.8 m_0$ [5] [42].

C. Band calculations

Numerical emulation of a regime as dilute as the one explored experimentally requires unrealistically large supercells. Therefore, a quantitative and microscopic explanation of the observed difference is challenging. However, considerable insight can be gained from DFT calculations. To this end, we used the projected augmented wave pseudo-potential code VASP [43] to fully optimize the crystal structure, including the lattice parameters, in the $8 \times 8 \times 8$ supercell of 64 formula units.

In the ground state, at $T = 0$, SrTiO_3 forms a tetragonal $I4/mcm$ structure, characterized with alternating rotations of the TiO_6 octahedra around the c axis. This is a strong effect well captured by the standard DFT calculations (Fig. 5). Proper stacking of the rotations along c , however, is quite difficult to obtain, and requires sophisticated setups. Our calculations, using standard PBE pseudopotentials, and up to $3 \times 3 \times 3$ mesh in the Brillouin zone, reproduce the rotations well, but form a different stacking, corresponding to a $P4/m$ group. The difference is not relevant for our analysis.

Since the optimized structure is tetragonal, there are two crystallographically nonequivalent sites, one preserving the tetragonal symmetry (we shall call it v-T) and the other lowering it to an orthorhombic one (v-O). In our calculations, the former corresponds to the space group $P4/m$ (incidentally, removal of Nb also results in the same symmetry), and the latter to $Pmm2$. At the level of our accuracy we could not determine with certainty which vacancy position is energetically preferable (see the supplement [35] for details).

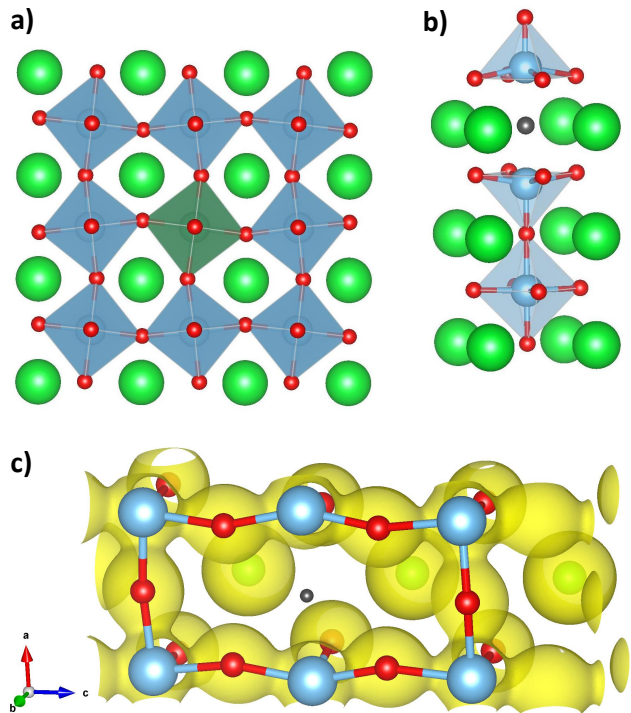


FIG. 5. **Effect of impurities on the crystal structure and electron density:**a) Crystal structure with a Nb impurity (green octahedron) b) Same for an O vacancy (black ball) preserving the tetragonal symmetry. c) The electron charge distribution around the vacancy; here the red balls are O, the blue-grey ones Ti and Sr are green. The black ball indicates the approximate location of the vacancy. The (yellow) isosurfaces are drawn at the level of electron density of $0.05 e/\text{\AA}^3$.

However, we were able to make one structural observation: both Nb and v-T case can be optimized with a

restriction forbidding octahedra rotations (v-O cannot). In the undoped compound these rotations decrease the total energy by 3.4 meV per formula. This energy difference increases, in our supercell, to 4.7 meV for Nb substitution. In contrast, it decreases to 0.9 meV for O vacancy. As discussed in the next section, this trend is in agreement with previous experimental findings.

The difference in the electronic structure (Fig. 6) is even more spectacular. Nb doping has little effect on the band dispersions, but the O vacancies dramatically modifies them. In case of v-T, the main effect is the relative shift between the two lower (xz and yz) bands and the upper (xy) band. This can be understood by analyzing the change of the local crystal field. As Fig. 5 shows, Nb introduces no visible additional distortion, while the vacancy alters the local environment of the two neighboring Ti from octahedral to pyramidal, and leads to a visible relaxations of the eight closest oxygen atoms.

Neglecting the small distortion of the octahedra, at the Γ point, which is the only one of interest, the hybridization of a Ti t_{2g} orbital with the four neighboring O atoms cancels out by symmetry (Fig. 7). However, if one apical oxygen is removed, the ligand field of the opposite one is uncompensated, so the corresponding band state is pushed up. In our case, this means that the xz and yz bands will be pushed up closer to the (unaffected) xy band at the Γ point (but not at the Z point). Of course, given the delocalization of the doped electrons, the effect on the entire band is reduced compared to the actual change of the site-local crystal field, but it still rather large on the scale of interest (i.e., ~ 10 meV). Note that no extra electron density is found in the calculations near the vacancy site (Fig. 7).

The situation for a v-O vacancy is more complicated. Qualitatively, the perturbation of the Ti environment is the same as depicted in Fig. 7b, but the picture needs to be rotated by 90° . Now it is not the xy orbitals that is being push down with respect to the other two, but yz . Since the xz/yz degeneracy with xy is already broken due to octahedra rotation, it leads to an interesting situation when the states at Γ are threefold split already on the nonrelativistic level, *i.e.*, without spin-orbit.

Interestingly, the calculated threshold for the first Lifshitz transition in the pristine crystal [30] is $n_{c1} = 6.4 \times 10^{17} \text{cm}^{-3}$. This is in quantitative agreement with what we find experimentally for $\text{SrTi}_{1-x}\text{Nb}_x\text{O}_3$ ($n_{c1} = 6.5 \pm 2 \times 10^{17} \text{cm}^{-3}$; Fig.4a), confirming that the rigid band approximation holds in this case (but not in $\text{SrTiO}_{3-\delta}$).

III. Discussion

Pristine strontium titanate goes through a cubic-to-tetragonal structural phase transition [44] at $T_s \simeq 105$ K. This is a (remarkably) second-order [45] structural phase transition driven by the softening of a Transverse Acoustic (TA) mode at the zone boundary [46]. Previous experiments have found that T_s increases by Nb substitution

and decreases by oxygen deficiency [47, 48]. In oxygen-reduced samples with a carrier density of 0.5% per formula unit, T_s drops by ~ 10 K [47]. In Nb-doped samples with a carrier density of 1% per formula unit, T_s increases by ~ 20 K [48]. This implies that the effect of the two doping routes on the boundary TA mode. This trend is reproduced by our DFT calculations. They found, as reported in the previous section, that the energy difference between the cubic and the tetragonal structures is amplified by Nb substitution and diminished by oxygen removal. Given the link between T_s and energy difference, our calculations provide a qualitative account of the experimental observation.

Interestingly, the softening of another soft phonon a Transverse Optical (TO) mode, located at the center of the Brillouin zone, would lead to ferroelectricity. This mode is suspected to play a prominent role in driving the superconducting instability in the dilute limit [23–27]. Given the contrasting consequences of the two doping routes for the boundary TA phonon (see above), one may wonder what would be their effect on the zone-centered ones. The dispersion of these TO phonons has been found to evolve with doping [7, 49]. But there is no record of a comparative study of their evolution in oxygen-reduced and Nb-substituted samples. Future studies may discriminate between the fingerprints of the two doping routes.

The present study reveals the contrasting outcomes of Nb substitution and oxygen reduction for metallicity and superconductivity. As we saw, the experimental data reveals a difference in the Fermi surface geometry in the two cases near the first Lifshitz transition. This is in qualitative agreement with our DFT calculations. They show that the band dispersion is different in the two cases. This agreement constitutes a ‘proof of the concept’. A quantitative confrontation between theory and experiment is beyond what can be achieved by the state-of-the-art. Indeed, the theoretical supercell is equivalent to a doping concentration of $\sim 10^{-2}$ per formula unit. This exceeds by two orders of magnitude the experimental one and impedes a direct comparison.

Let us note that very recently, Tomioka *et al.* [31] have confirmed that below a threshold density of $\approx 8 \times 10^{18} \text{cm}^{-3}$, $\text{SrTi}_{1-x}\text{Nb}_x\text{O}_3$ and $\text{Sr}_{1-x}\text{La}_x\text{TiO}_3$ do not superconduct. On the other hand, replacing Sr with either Ca or Ba makes them superconducting. This provides additional support for dopant dependent superconductivity in the dilute limit and calls for an experimental study of the fermiology in polar metals such as $\text{Nb}:\text{Sr}_{0.985}\text{Ca}_{0.015}\text{TiO}_3$.

Dopant-dependent superconductivity has been reported in other cases. Beyond a critical threshold of Tl doping, $\text{Pb}_{1-x}\text{Tl}_x\text{Te}$ is a superconductor, but $\text{Pb}_{1-x}\text{Na}_x\text{Te}$ is non-superconducting [50, 51]. The difference has been tracked to the presence of Tl impurity states near the Fermi energy. Let us note that the concentration of dopants is two orders of magnitude lower in strontium titanate than in lead telluride. The exper-

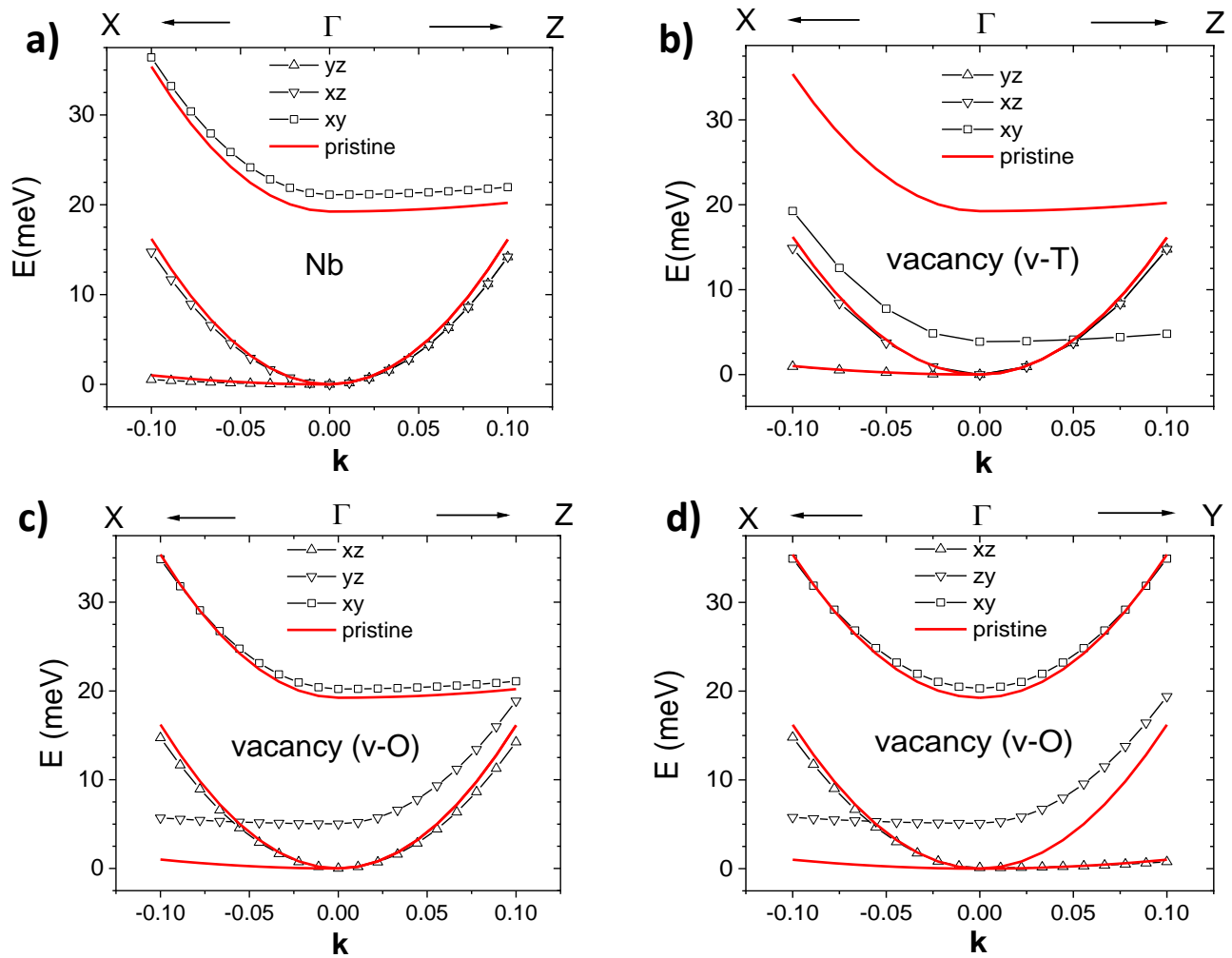


FIG. 6. Non-relativistic band states in $\text{Sr}_{64}\text{Ti}_{63}\text{NbO}_{192}$ (a) and in $\text{Sr}_{64}\text{Ti}_{64}\text{O}_{191}$ (b,c,d). In all cases, the structure was fully optimized within DFT. Only in the case of Nb substitution, the dispersion is virtually identical to the pristine case. In (b), the oxygen vacancy (v-T) keeps the tetragonal symmetry of the lattice. In (c) and (d), the oxygen vacancy (v-O) makes the system orthorhombic and as seen in (d) the dispersion along x- and y-axes are no more identical. The horizontal axis refers to distances in the momentum space along different orientations expressed in reciprocal lattice units.

imental observation of dopant dependent superconductivity has motivated theoretical scenarios [52, 53], which may be relevant to our result. Nevertheless, large Hubbard correlations are unlikely in the extreme dilute limit. Occam's razor [54] would favor scenarios which do not require them.

Thus, like lead telluride, strontium titanate demonstrate that the rigid band approximation does not capture the whole physics when a small concentration of dopants turns a solid off-stoichiometric. Future studies will tell if the breakdown of the rigid band approximation has any visible signature in the thermoelectric response [55], as found in the case of PbTe [56], where doping by Tl has led to an amplification of the thermoelectric figure of merit.

Thus, like lead telluride, strontium titanate demon-

strate that the rigid band approximation does not capture the whole physics when a small concentration of dopants turns a solid off-stoichiometric solids. Future studies will tell if the breakdown of the rigid band approximation has any visible signature in the thermoelectric response [55], as found in the case of PbTe [56], where doping by Tl has led to an amplification of the thermoelectric figure of merit.

In summary, we found that doping strontium titanate by removing oxygen leads to a dilute metal different from the one obtained by substituting Ti with Nb. The two detected differences are the band dispersion and the presence and absence of a superconducting instability. The exceptionally dilute superconductivity is an instability in a band specifically sculpted by oxygen vacancies of strontium titanate.

IV. Materials and methods

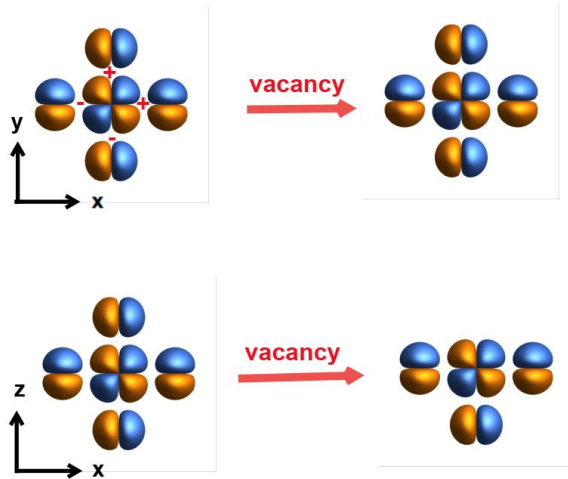


FIG. 7. Effect of a “tetragonal” v-O vacancy on the ligand crystal field Relevant Ti d and O p wave functions for the wave vector \mathbf{k} corresponding to the Γ point, in the real space around a Ti site. In absence of O vacancy, the hybridization of all t_{2g} orbitals with the O states cancels out by symmetry. Introducing a vacancy does not change this for the xy orbital (top) but the cancellation is broken by the vacancy for the xz and yz (not shown) orbitals (bottom). As a consequence, in the momentum space, the corresponding bands at the Γ point shift upward.

Nb-doped films were synthesized on SrTiO₃ (001) substrate in pulsed laser deposition, as detailed previously [34, 57]. Oxygen-deficient SrTiO₃ single crystals were obtained by annealing commercially bought substrates in a manner similar to what was described in ref.[5, 29, 58]. Four-contact resistivity measurements were performed in a dilution refrigerator inserted in a 17 T superconducting magnet.

Band calculations used the Projector Augmented Wave method together with the Generalized Gradient Correction to the exchange-correlation potential [59], as implemented in the VASP package [43]. Fig. 5 was generated using the VESTA program [60].

V. Acknowledgements

We thank Claude Ederer and Maria Gastiasoro for useful discussions.

This work was supported by the Agence Nationale de la Recherche (ANR-18-CE92-0020-01; ANR-19-CE30-0014-04), by Jeunes Equipes de l’Institut de Physique du Collège de France and by a grant attributed by the Ile de France regional council. It was funded in part by a QuantEmX grant from ICAM and the Gordon and Betty Moore Foundation through Grant GBMF9616 to KB. The work at SLAC/Stanford is supported by the U.S. Department of Energy, Office of Basic Energy Sciences, Division of Materials Sciences and Engineering, under Contract No. DE-AC02-76SF00515.

-
- [1] J. F. Schooley, W. R. Hosler, and M. L. Cohen, Superconductivity in semiconducting SrTiO₃, Phys. Rev. Lett. **12**, 474 (1964).
 - [2] C. Collignon, X. Lin, C. W. Rischau, B. Fauqué, and K. Behnia, Metallicity and superconductivity in doped strontium titanate, Annual Review of Condensed Matter Physics **10**, 25 (2019).
 - [3] M. N. Gastiasoro, J. Ruhman, and R. M. Fernandes, Superconductivity in dilute SrTiO₃: A review, Annals of Physics **417**, 168107 (2020).
 - [4] G. M. Eliashberg, Interactions between electrons and lattice vibrations in a superconductor, Sov. Phys. - JETP **11**, 696 (1960).
 - [5] X. Lin, Z. Zhu, B. Fauqué, and K. Behnia, Fermi surface of the most dilute superconductor, Phys. Rev. X **3**, 021002 (2013).
 - [6] H. Yoon, A. G. Swartz, S. P. Harvey, H. Inoue, Y. Hikita, Y. Yu, S. B. Chung, S. Raghu, and H. Y. Hwang, Low-density superconductivity in SrTiO₃ bounded by the adiabatic criterion, arXiv e-prints, arXiv:2106.10802 (2021).
 - [7] C. Collignon, P. Bourges, B. Fauqué, and K. Behnia, Heavy nondegenerate electrons in doped strontium titanate, Phys. Rev. X **10**, 031025 (2020).
 - [8] A. Kumar, V. I. Yudson, and D. L. Maslov, Quasiparticle and nonquasiparticle transport in doped quantum paraelectrics, Phys. Rev. Lett. **126**, 076601 (2021).
 - [9] K. G. Nazaryan and M. V. Feigel'man, Conductivity and thermoelectric coefficients of doped SrTiO₃ at high temperatures, Phys. Rev. B **104**, 115201 (2021).
 - [10] C. Collignon, Y. Awashima, Ravi, X. Lin, C. W. Rischau, A. Acheche, B. Vignolle, C. Proust, Y. Fuseya, K. Behnia, and B. Fauqué, Quasi-isotropic orbital magnetoresistance in lightly doped SrTiO₃, Phys. Rev. Materials **5**, 065002 (2021).
 - [11] K. A. Müller and H. Burkard, SrTiO₃: An intrinsic quantum paraelectric below 4 k, Phys. Rev. B **19**, 3593 (1979).
 - [12] V. Martelli, J. L. Jiménez, M. Continentino, E. Baggio-Saitovitch, and K. Behnia, Thermal transport and phonon hydrodynamics in strontium titanate, Phys. Rev. Lett. **120**, 125901 (2018).
 - [13] X. Li, B. Fauqué, Z. Zhu, and K. Behnia, Phonon thermal hall effect in strontium titanate, Phys. Rev. Lett. **124**, 105901 (2020).
 - [14] X. He, D. Bansal, B. Winn, S. Chi, L. Boatner, and O. Delaire, Anharmonic eigenvectors and acoustic phonon disappearance in quantum paraelectric SrTiO₃, Phys. Rev. Lett. **124**, 145901 (2020).
 - [15] B. Fauqué, P. Bourges, A. Subedi, K. Behnia, B. Bap-

- tiste, B. Roessli, T. Fennell, S. Raymond, and P. Steffens, Mesoscopic fluctuating domains in strontium titanate, *Phys. Rev. B* **106**, L140301 (2022).
- [16] S. E. Rowley, L. J. Spalek, R. P. Smith, M. P. M. Dean, M. Itoh, J. F. Scott, G. G. Lonzarich, and S. S. Saxena, Ferroelectric quantum criticality, *Nature Physics* **10**, 367 (2014).
- [17] J. M. Edge, Y. Kedem, U. Aschauer, N. A. Spaldin, and A. V. Balatsky, Quantum critical origin of the superconducting dome in SrTiO₃, *Phys. Rev. Lett.* **115**, 247002 (2015).
- [18] C. Enderlein, J. F. de Oliveira, D. A. Tompsett, E. B. Saitovitch, S. S. Saxena, G. G. Lonzarich, and S. E. Rowley, Superconductivity mediated by polar modes in ferroelectric metals, *Nature Communications* **11**, 4852 (2020).
- [19] C. W. Rischau, X. Lin, C. P. Grams, D. Finck, S. Harms, J. Engelmayer, T. Lorenz, Y. Gallais, B. Fauqué, J. Hemberger, and K. Behnia, A ferroelectric quantum phase transition inside the superconducting dome of Sr_{1-x}Ca_xTiO_{3-d}, *Nature Physics* **13**, 643 (2017).
- [20] Y. Tomioka, N. Shirakawa, K. Shibuya, and I. H. Inoue, Enhanced superconductivity close to a non-magnetic quantum critical point in electron-doped strontium titanate, *Nature Communications* **10**, 738 (2019).
- [21] K. Ahadi, L. Galletti, Y. Li, S. Salmani-Rezaie, W. Wu, and S. Stemmer, Enhancing superconductivity in SrTiO₃ films with strain, *Science Advances* **5**, eaaw0120 (2019), <https://www.science.org/doi/pdf/10.1126/sciadv.aaw0120>.
- [22] C. W. Rischau, D. Pulmannová, G. W. Scheerer, A. Stucky, E. Giannini, and D. van der Marel, Isotope tuning of the superconducting dome of strontium titanate, *Phys. Rev. Research* **4**, 013019 (2022).
- [23] D. van der Marel, F. Barantani, and C. W. Rischau, Possible mechanism for superconductivity in doped SrTiO₃, *Phys. Rev. Research* **1**, 013003 (2019).
- [24] D. E. Kiselev and M. V. Feigel'man, Theory of superconductivity due to ngai's mechanism in lightly doped SrTiO₃, *Phys. Rev. B* **104**, L220506 (2021).
- [25] P. A. Volkov, P. Chandra, and P. Coleman, Superconductivity from energy fluctuations in dilute quantum critical polar metals, *Nature Communications* **13**, 4599 (2022).
- [26] M. N. Gastiasoro, M. E. Temperini, P. Barone, and J. Lorenzana, Theory of superconductivity mediated by rashba coupling in incipient ferroelectrics, *Phys. Rev. B* **105**, 224503 (2022).
- [27] Y. Yu, H. Y. Hwang, S. Raghu, and S. B. Chung, Theory of superconductivity in doped quantum paraelectrics, *npj Quantum Materials* **7**, 63 (2022).
- [28] K. L. Ngai, Two-phonon deformation potential and superconductivity in degenerate semiconductors, *Phys. Rev. Lett.* **32**, 215 (1974).
- [29] X. Lin, G. Bridoux, A. Gourgout, G. Seyfarth, S. Krämer, M. Nardone, B. Fauqué, and K. Behnia, Critical doping for the onset of a two-band superconducting ground state in SrTiO_{3-δ}, *Phys. Rev. Lett.* **112**, 207002 (2014).
- [30] D. van der Marel, J. L. M. van Mechelen, and I. I. Mazin, Common fermi-liquid origin of T^2 resistivity and superconductivity in n -type SrTiO₃, *Phys. Rev. B* **84**, 205111 (2011).
- [31] Y. Tomioka, N. Shirakawa, and I. H. Inoue, Superconductivity enhancement in polar metal regions of Sr_{0.95}Ba_{0.05}TiO₃ and Sr_{0.985}Ca_{0.015}TiO₃ revealed by systematic Nb doping, *npj Quantum Materials* **7**, 111 (2022).
- [32] Z. Hou and K. Terakura, Defect states induced by oxygen vacancies in cubic srtio3: First-principles calculations, *Journal of the Physical Society of Japan* **79**, 114704 (2010), <https://doi.org/10.1143/JPSJ.79.114704>.
- [33] J. Souto-Casares, N. A. Spaldin, and C. Ederer, Oxygen vacancies in strontium titanate: A DFT + DMFT study, *Phys. Rev. Research* **3**, 023027 (2021).
- [34] Y. Kozuka, Y. Hikita, C. Bell, and H. Y. Hwang, Dramatic mobility enhancements in doped SrTiO₃ thin films by defect management, *Applied Physics Letters* **97**, 012107 (2010).
- [35] See Supplemental Material for more details and additional data regarding the samples and the methods.
- [36] X. Lin, A. Gourgout, G. Bridoux, F. m. c. Jomard, A. Pourret, B. Fauqué, D. Aoki, and K. Behnia, Multiple nodeless superconducting gaps in optimally doped sr_{t1-x}nb_xo₃, *Phys. Rev. B* **90**, 140508 (2014).
- [37] C. Collignon, B. Fauqué, A. Cavanna, U. Gennser, D. Mailly, and K. Behnia, Superfluid density and carrier concentration across a superconducting dome: The case of strontium titanate, *Phys. Rev. B* **96**, 224506 (2017).
- [38] K. Szot, W. Speier, R. Carius, U. Zastrow, and W. Beyer, Localized metallic conductivity and self-healing during thermal reduction of SrTiO₃, *Phys. Rev. Lett.* **88**, 075508 (2002).
- [39] K. Behnia, On mobility of electrons in a shallow fermi sea over a rough seafloor, *Journal of Physics: Condensed Matter* **27**, 375501 (2015).
- [40] H. Uwe, R. Yoshizaki, T. Sakudo, A. Izumi, and T. Uzu-maki, Conduction band structure of SrTiO₃, *Japanese Journal of Applied Physics* **24**, 335 (1985).
- [41] S. J. Allen, B. Jalan, S. Lee, D. G. Ouellette, G. Khalsa, J. Jaroszynski, S. Stemmer, and A. H. MacDonald, Conduction-band edge and shubnikov-de haas effect in low-electron-density SrTiO₃, *Phys. Rev. B* **88**, 045114 (2013).
- [42] The lower band is non-parabolic [30], and therefore, the effective mass is expected to increase with increasing carrier density. Experimentally, m^* in the oxygen-doped samples becomes $\approx 3.5 m_0$ at $n_H = 3 \times 10^{19} \text{cm}^{-3}$ [29].
- [43] G. Kresse and J. Hafner, Ab initio molecular dynamics for liquid metals, *Phys. Rev. B* **47**, 558 (1993).
- [44] F. W. Lytle, X-ray diffractometry of low-temperature phase transformations in strontium titanate, *Journal of Applied Physics* **35**, 2212 (1964).
- [45] E. K. H. Salje, M. C. Gallardo, J. Jiménez, F. J. Romero, and J. del Cerro, The cubic-tetragonal phase transition in strontium titanate: excess specific heat measurements and evidence for a near-tricritical, mean field type transition mechanism, *Journal of Physics: Condensed Matter* **10**, 5535 (1998).
- [46] G. Shirane and Y. Yamada, Lattice-dynamical study of the 110°k phase transition in SrTiO₃, *Phys. Rev.* **177**, 858 (1969).
- [47] D. Bäuerle and W. Rehwald, Structural phase transitions in semiconducting SrTiO₃, *Solid State Communications* **27**, 1343 (1978).
- [48] Q. Tao, B. Loret, B. Xu, X. Yang, C. W. Rischau, X. Lin, B. Fauqué, M. J. Verstraete, and K. Behnia, Nonmonotonic anisotropy in charge conduction induced by antiferrodistortive transition in metallic sr_{tio3}, *Phys. Rev. B* **94**, 035111 (2016).
- [49] W. Rehwald, Low temperature elastic moduli of stron-

- tium titanate, *Solid State Communications* **8**, 1483 (1970).
- [50] Y. Matsushita, H. Bluhm, T. H. Geballe, and I. R. Fisher, Evidence for charge kondo effect in superconducting tl-doped PbTe, *Phys. Rev. Lett.* **94**, 157002 (2005).
- [51] P. Giraldo-Gallo, P. Walmsley, B. Sangiorgio, S. C. Riggs, R. D. McDonald, L. Buchauer, B. Fauqué, C. Liu, N. A. Spaldin, A. Kaminski, K. Behnia, and I. R. Fisher, Evidence of incoherent carriers associated with resonant impurity levels and their influence on superconductivity in the anomalous superconductor $\text{Pb}_{1-x}\text{Tl}_x\text{Te}$, *Phys. Rev. Lett.* **121**, 207001 (2018).
- [52] M. Dzero and J. Schmalian, Superconductivity in charge kondo systems, *Phys. Rev. Lett.* **94**, 157003 (2005).
- [53] S. A. Kivelson, Physics of superconducting transition temperatures, *Journal of Superconductivity and Novel Magnetism* **33**, 5 (2020).
- [54] I. Mazin, Inverse Occam's razor, *Nature Physics* **18**, 367 (2022).
- [55] M.-S. Lee and S. D. Mahanti, Validity of the rigid band approximation in the study of the thermopower of narrow band gap semiconductors, *Phys. Rev. B* **85**, 165149 (2012).
- [56] J. P. Heremans, V. Jovovic, E. S. Toberer, A. Saramat, K. Kurosaki, A. Charoenphakdee, S. Yamanaka, and G. J. Snyder, Enhancement of thermoelectric efficiency in pbte by distortion of the electronic density of states, *Science* **321**, 554 (2008), <https://www.science.org/doi/pdf/10.1126/science.1159725>.
- [57] H. Inoue, H. Yoon, T. A. Merz, A. G. Swartz, S. S. Hong, Y. Hikita, and H. Y. Hwang, Delta-doped SrTiO₃ top-gated field effect transistor, *Applied Physics Letters* **114**, 231605 (2019).
- [58] A. Spinelli, M. A. Torija, C. Liu, C. Jan, and C. Leighton, Electronic transport in doped SrTiO₃: Conduction mechanisms and potential applications, *Phys. Rev. B* **81**, 155110 (2010).
- [59] J. P. Perdew, K. Burke, and M. Ernzerhof, Generalized gradient approximation made simple, *Phys. Rev. Lett.* **77**, 3865 (1996).
- [60] K. Momma and F. Izumi, *VESTA3* for three-dimensional visualization of crystal, volumetric and morphology data, *Journal of Applied Crystallography* **44**, 1272 (2011).

Supplementary Material

S1. Samples

The present study compared the fermiology and the superconducting transition in thin films of $\text{SrTi}_{1-x}\text{Nb}_x\text{O}_3$ and in single crystals of $\text{SrTiO}_{3-\delta}$.

Nb-doped films were synthesized on SrTiO_3 (001) substrate in pulsed laser deposition. A cap and buffer layer were used to prevent surface depletion in the doped layer [55]. The growth recipes were described previously, resulting in a similar carrier density and mobility of films to those of bulk crystals [34]. Particularly for S4, we repetitively switched two targets of 0.02 at.% of Nb and undoped to synthesize the lower carrier density than the nominal density of the Nb target. In order to keep the uniform dopant distribution avoiding the effects of superlattices, the pulse number for a single period (6 pulses for Nb-doped, 6 pulsed for undoped) was intentionally set to be lower than the pulse number needed for growing one unit cell (16 pulses).

Oxygen-deficient SrTiO_3 samples were obtained by annealing commercially bought substrates in an oven in a temperature range of 700°C to 1000°C under vacuum ($< 10^{-6}$ mbar) [29,56].

Sample	μ_H ($\text{V}\cdot\text{cm}^{-2}\cdot\text{s}^{-1}$)	n_H (cm^{-3})	F_1 (T)	F_2 (T)	dopant	thickness (nm)	Undoped cap layer (nm)
S_1	4100	$4.4\text{e}18$	36	137	0.04 at.% Nb	892	119
S_2	3162	$1.65\text{e}18$	16	72	0.02 at.% Nb	617	102
S_3	1365	$1.5\text{e}18$	14	58	0.02 at.% Nb	895	90
S_4	9084	$8.6\text{e}17$	9	33	0.02 at.% Nb	748	100

TABLE S1. $\text{SrTi}_{1-x}\text{Nb}_x\text{O}_3$ thin films studied in this workd and their properties- Carrier densities and Hall mobilities are given at 2 K.

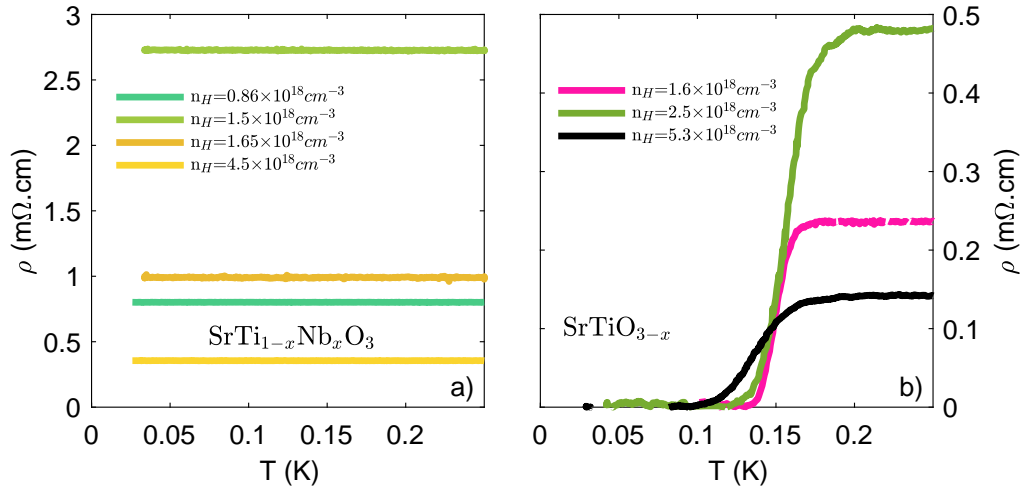


FIG. S1. **Low temperature resistivity revealing a difference in the ground state for the two doping routes-** Resistivity, ρ , in $\text{SrTi}_{1-x}\text{Nb}_x\text{O}_3$ (a) and in $\text{SrTiO}_{3-\delta}$ (b), when Hall carrier densities range from 10^{18} cm^{-3} to $5 \times 10^{18} \text{ cm}^{-3}$. SrTiO_{3-x} is a superconductor and $\text{SrTi}_{1-x}\text{Nb}_x\text{O}_3$ is not.

S2. Reproducibility

Tab.S1 lists the electronic properties of the four Nb thin film samples studied. At low temperature, none of these samples display a superconducting transition. This is in sharp contrast with oxygen-reduced samples of similar Hall carrier density (see Fig.S1).

As discussed in the main text, this difference is concomitant with a difference in the Fermi surface geometries. Fig. S2 shows the trace of the quantum oscillations and its Fourier Transform for the four Nb-doped samples. In all samples, two main frequencies, labelled F_1 and F_2 , are detected as well as their harmonics. The evolution of F_1 and F_2 with doping is shown in Fig.3 of the main manuscript.

As one can see, in all these samples there is more than one frequency. The higher frequency, which corresponds to the lower filled band or the outer Fermi surface pocket, is only detectable at higher fields and therefore its detection by a Fourier transform requires to restrict the analysis to a higher field window.

S3. Calculations

We used the Projector Augmented Wave method in conjunction with the Generalized Gradient Correction to the exchange-correlation potential [57], as implemented in the VASP package [43]. We used an 8x8x8 quasi-cubic supercell to emulate either defect. Gaussian smearing with $\sigma = 20$ meV was used, and the k -point mesh was 2x2x2. The plane-wave cutoff was 400 eV. Note that full structural optimization was performed, as opposed to Ref. [30], where the experimental low-temperature structure was used (the latter approach is more accurate, but not possible for the doped cases).

The resulting structures can be downloaded as Supplementary files Sr64NbTi63O192.cif and Sr64Ti64O191.cif. Visualization used in Fig. 5 in the main text was generated using the VESTA program [58].

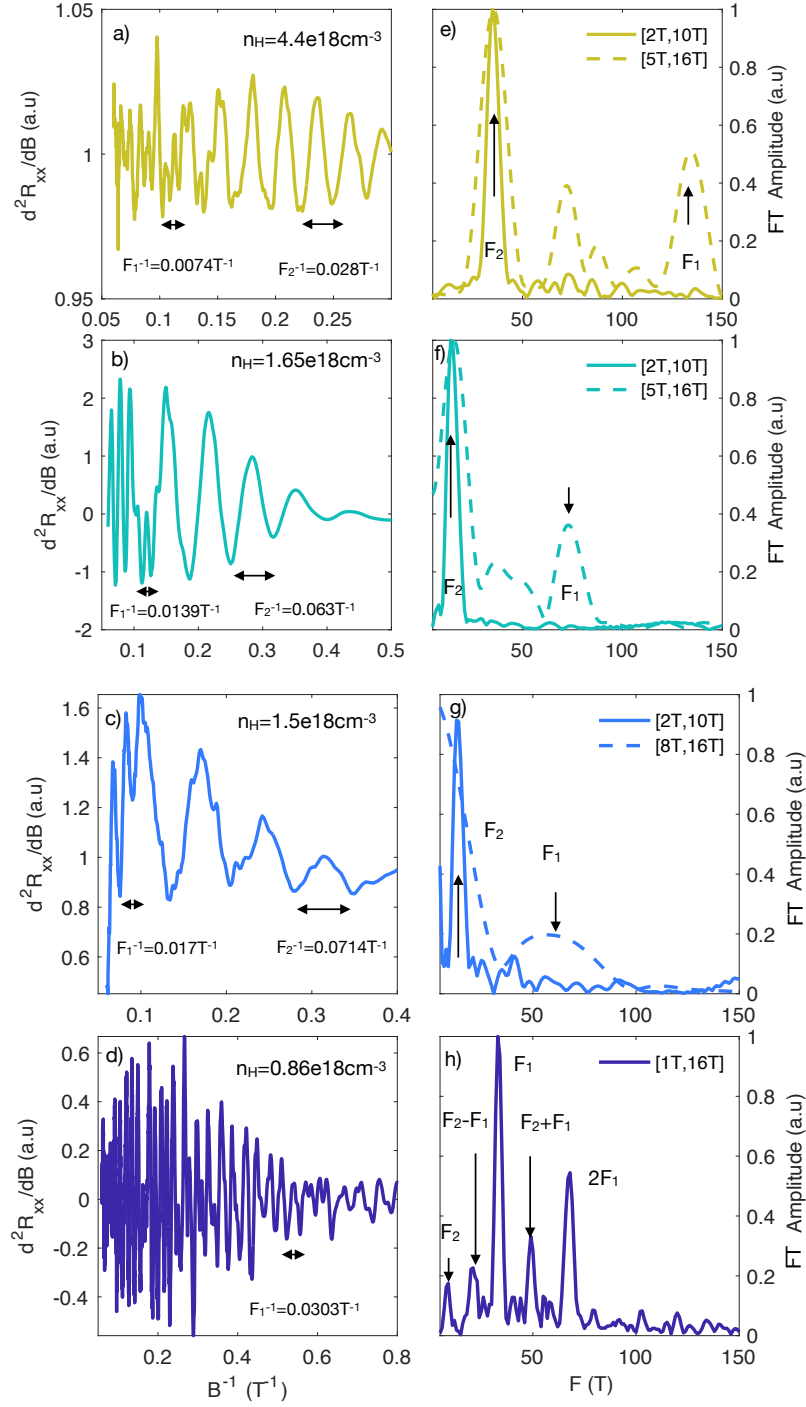


FIG. S2. **Extended quantum oscillations data** a)-d) $\frac{\partial^2 R_{xx}}{\partial B^2}$ as a function of the inverse of the magnetic field in the four $SrTi_{1-x}Nb_xO_3$ samples studied at low temperature. e-h) Normalised amplitudes of the Fourier transform deduced from a)-d). In three cases, two different magnetic field windows were used for performing Fourier transform to highlight the emergence of a second frequency at high magnetic field.